Dynamics Study of the HO(v'=0) + O_2(v'') Branching Atmospheric Reaction. 1. Formation of Hydroperoxyl Radical

J. D. Garrido,† P. J. S. B. Caridade, and A. J. C. Varandas*

Departamento de Química, Universidade de Coimbra, P-3049 Coimbra, Portugal

Received: March 3, 1999; In Final Form: April 19, 1999

We report a theoretical study of the title four-atom atmospheric reaction for a range of translational energies $0.1 \le E_{tr}$/kcal mol$^{-1} \le 40$ and the range $13 \le v'' \le 27$ of vibrational quantum numbers of the oxygen molecule. All calculations have employed the quasiclassical trajectory method, and a realistic potential energy surface obtained by using the double many-body expansion (DMBE) method for ground-state HO_3.

1. Introduction

The hydrogen−oxygen systems are very important in atmospheric chemistry,[1,2] combustion chemistry,[3] and laser processes.[4] In particular, the reaction

$$H + O_3 \rightarrow HO(v) + O_2 \quad (1)$$

which is a source of vibrationally excited HO($v \le 9$), has been extensively studied.[5−18] Moreover, several theoretical and experimental results on the quenching of HO(v') in collisions with Ar,[19,20] N_2,[21] CO_2,[22] and O_2[22,23] have been reported. In addition, an aborted chemical reaction mechanism has been proposed[23] to explain the high efficiency in the relaxation process of HO(v') by O_2, the authors having utilized for this purpose their own model of the potential energy surface for ground-state HO_3. From this work, Shalashilin *et al.*[23] have conjectured that the reaction

$$HO + O_2 \rightarrow HO_2 + O \quad (2)$$

is not dominant, and recognized that it is an open problem that requires further study. Moreover, although lying energetically higher, there is another possible reactive channel leading to ozone formation

$$HO + O_2 \rightarrow O_3 + H \quad (3)$$

Thus, the HO + O_2 reaction may provide an interesting example of a multichannel reactive process whose outcoming products may be controlled through appropriate selection of the energy contents of the reactant species. This topic will be explored in this and subsequent publications, as well as the vibrational relaxation process. In summary, the title reaction in its most generalized form HO(v') + O_2(v'') may be a potential source of both HO_2 and O_3, which are vital natural species in atmospheric chemistry.

A major goal of the present work is therefore to report a detailed theoretical study of the title branching reaction

$$HO(v'=0) + O_2(v'') \rightarrow HO_2 + O \quad (4)$$

by using the quasiclassical trajectory (QCT) method and a recently reported[24] single-valued double many-body expansion (DMBE) potential energy surface for the electronic ground state of HO_3; throughout the paper, the absence of a specific vibrational state in the reactants implies that the corresponding species is in its ground vibrational state, *e.g.*, HO ≡ HO(v'=0). It should be noted that the HO_3 DMBE potential energy surface has been extensively used to study the inverse title reaction[25,26]

$$HO_2 + O \rightarrow HO + O_2 \quad (5)$$

and the reverse of the reaction 3.[27−29] In both cases there was good agreement with the available experimental data.

The paper is organized as follows. Section 2 provides a brief survey of the HO_3(^{2}A) DMBE potential energy surface, while the computational method is described in section 3. The results are presented and discussed in section 4, while the major conclusions are in section 5.

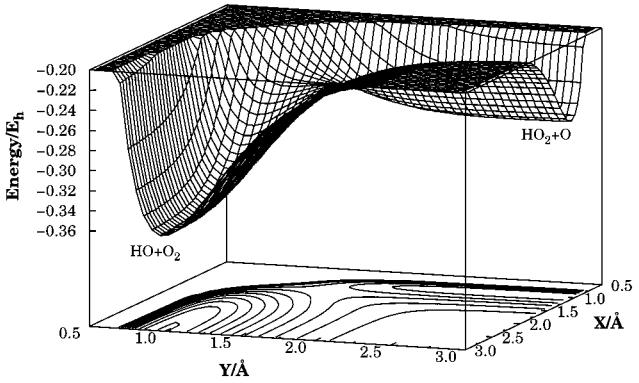

Figure 1. A perspective plot of the potential energy surfaces for the reaction HO(v') + O_2(v'') → HO_2 + O.

2. Potential Energy Surface

All calculations reported in this work have employed a six-dimensional (6D) DMBE potential energy surface[24] for the electronic ground state of HO_3. Since it has been described in detail elsewhere,[24] we focus here on its main topographical features which are of interest for the title reaction.

Figure 1 shows a perspective view of the HO_3 potential energy surface for the regions of configurational space with relevance for the studied reaction. The *x*-axis represents the

† Permanent address: Departamento de Física General y Matemática, Instituto Superior de Ciencias y Tecnología Nucleares, 6163 Havana, Cuba.

10.1021/jp990756o CCC: $18.00
Published on Web 06/06/1999

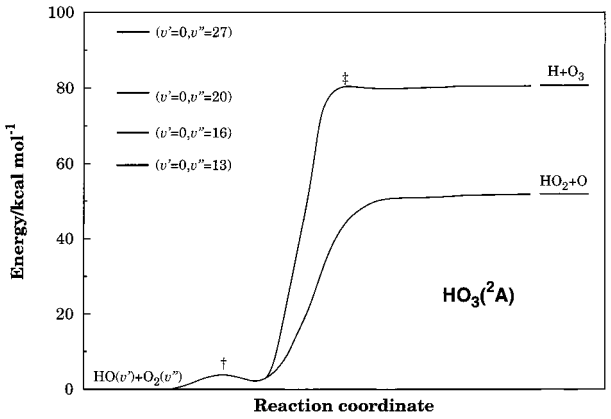

Figure 2. Minimum energy path for formation of $HO_2 + O$ and $O_3 + H$. Shown by the symbols † and ‡ are the saddle points for the $H + O_3 \rightarrow OH + O_2$ and $HO_2 + O \rightarrow OH + O_2$ processes, respectively. Also shown are some vibrational energy levels of the two reactant molecules.

O−O distance between one atom of the incoming oxygen molecule and the oxygen of the HO radical, while the *y*-axis denotes the distance between the oxygen atoms in the oxygen molecule. Note that the ∠OOO, ∠HOO, and ∠HOOO torsion angles as well as the H−O distance have been partially relaxed ($112.7 \leq \theta_{OOO}/\text{deg} \leq 118.7$, $94.6 \leq \theta_{HOO}/\text{deg} \leq 104.3$, $82.6 \leq \phi_{HOOO}/\text{deg} \leq 90.6$, $0.9708 \leq R_{HO}/\text{Å} \leq 1.0315$) in this plot. The calculated minimum energy reaction paths for the title reaction and the one leading to ozone formation are shown in Figure 2. Also shown in this figure is the energetics of the various combinations of vibrational quantum numbers according to the HO_3 DMBE potential energy surface. Note that the title reaction is feasible for the complete range of translational energies only for vibrational quantum numbers $v'' \geq 13$. However, for the case of ozone formation, such a reaction is energetically allowed only when the vibrational quantum number of the oxygen molecule is higher than $v'' = 22$.

3. Computational Procedures

The QCT method has been used in the present work to study the $HO(v') + O_2(v'')$ reaction. To run the classical trajectories we have utilized an extensively adapted version of the MERCURY[30] code which accommodates the HO_3 DMBE potential energy surface and makes the appropriate assignment of the reactive channels. Calculations have been carried for diatom−diatom translational energies in the range $0.1 \leq E_{tr}/\text{kcal mol}^{-1} \leq 40$, as specified in Table 1. In all cases the initial rotational quantum numbers of the colliding O_2 and HO molecules have been fixed at the ground level ($j_{HO} = j_{O_2} = 1$) and the HO molecule kept in its ground vibrational state. The determination of the step size for numerical integration has been done by trial and error on the basis of accuracy requirements. A value of 1.5×10^{-16} s has been found sufficient to warrant conservation of energy to better then 2 parts in 10^5. In turn, the diatomic−diatomic initial separation has been fixed at 8 Å, a value sufficiently large to make the interaction negligible. To select the maximum value of the impact parameter (b_{max}) which leads to reaction, we have followed the usual procedure by computing batches of 100 trajectories for fixed values of *b*. This procedure should allow an accuracy in b_{max} of about ±0.1 Å; the calculated values are reported in Table 1. Batches of 3000 trajectories have then been carried out for each translational energy and vibrational combination making a total of about 8×10^4 trajectories. Such a number of trajectories has been found enough to yield reactive cross sections with an error of typically a few percent.

For a specified translational energy, the reactive cross sections are given by

$$\sigma^r_{0v''} = \pi b^2_{max} P_{0v''} \tag{6}$$

and the associated 68% uncertainties are

$$\Delta\sigma^r_{0v''} = \left(\frac{N_{0v''} - N^r_{0v''}}{N_{0v''} N^r_{0v''}}\right)^{1/2} \sigma^r_{0v''} \tag{7}$$

where $N^r_{0v''}$ is the number of reactive trajectories in a total of $N_{0v''}$ for the combination $(0, v'')$ of the vibrational quantum numbers of the colliding molecules, and $P_{0v''} = N^r_{0v''}/N_{0v''}$ is the reactive probability. From the reactive cross section and assuming a Maxwell−Boltzmann distribution over the translational energy (E_{tr}), the specific thermal rate coefficients are obtained as

$$k_{0v''} = g_e(T) \left(\frac{2}{k_B T}\right)^{3/2} \left(\frac{1}{\pi\mu}\right)^{1/2} \int_0^\infty E_{tr} \sigma^r_{0v''} \exp\left(-\frac{E_{tr}}{k_B T}\right) dE_{tr} \tag{8}$$

where

$$g_e(T) = \frac{1}{3}\left[\frac{1}{1 + \exp(-205/T)}\right] \tag{9}$$

is the factor that accounts for the electronic degeneracies in the title reaction, k_B is the Boltzmann constant, μ is the reduced mass of the colliding diatomic particles, and *T* is the temperature.

4. Results and Discussion

Table 1 summarizes the trajectory calculations carried out for the $HO + O_2(v'')$ reaction. Column one of this table indicates the vibrational quantum number of the O_2 molecule while the studied translational energies are in column two. For these initial translational energies (with exception of the cases 20 and 40 kcal mol^{-1} for the combination (0,27)), the only open reactive channels are the following:

$$HO_a + O_bO_c(v'') \rightarrow HO_bO_c + O_a \tag{10}$$

$$\rightarrow HO_aO_c + O_b \tag{11}$$

$$\rightarrow HO_aO_b + O_c \tag{12}$$

where the indices *a*, *b*, and *c* label the three oxygen atoms. In the cases of indistinguishable atoms, the reactions in eq 11 and eq 12 have similar probabilities of occurrence. In turn, the probability of reaction 10 is very small (or zero), which may be attributed to the fact that the HO bond is very strong, especially in its ground vibrational level. Such a result is consistent with the findings reported in ref 25 in connection with the occurrence of the inverse reaction only via an oxygen-atom abstraction path. For the vibrational combination (0,27), with translational energies 20 and 40 kcal mol^{-1}, other channels become open as shown in Table 2.

4.1. Dynamical Features. Figure 3 shows the dependence of the maximum impact parameter with translational energy for the formation of HO_2. For vibrational quantum numbers $v'' = 16$ and 27, the value of b_{max} increases with decreasing translational energy while, for higher translational energies, b_{max} is essentially constant or slightly increases with E_{tr}. Thus, in the first case, we expect that HO_2 formation is dictated by a capture-type mechanism where long-range forces play an important role. Conversely, the second regime is more typical

TABLE 1: Summary of the Trajectory Calculations for Various Initial Vibrational States of O_2 Molecule[a]

			HO_2 + O formation				exchange reaction			
v''	E_{tr} (kcal mol^{-1})	b_{max} (Å^2)	N_r	$100P_r$	σ^r/Å^2	$100\Delta\sigma^r$/Å^2	N_r	$100P_r$	σ^r/Å^2	$100\Delta\sigma^r$/Å^2
13	1	1.9	13	0.44	0.05	1.4	2985	99.6	11.3	1.5
	5	2.0	41	1.36	0.17	2.7	2959	98.6	12.4	2.7
	10	2.4	54	1.80	0.33	4.4	2946	98.2	17.8	4.4
	15	2.45	139	4.64	0.88	7.2	2861	95.4	18.0	7.2
	20	2.65	157	5.24	1.16	0.1	2843	94.8	20.9	9.0
	30	2.75	262	8.74	2.08	12.2	2738	91.3	21.7	12.2
	40	2.85	423	14.10	3.60	16.2	2577	85.9	21.9	16.2
16	0.1	3.1	13	1.30	0.40	10.8	985	98.7	29.8	10.8
	1	2.4	46	1.53	0.28	4.1	2943	98.5	17.8	4.1
	5	3.1	49	1.64	0.50	5.2	2951	98.4	29.7	7.0
	7.5	2.9	99	3.30	0.87	8.6	2901	96.7	25.5	8.6
	10	2.75	115	3.84	0.90	8.3	2885	96.2	22.8	8.3
	15	2.95	165	5.51	1.50	11.4	2835	94.5	25.8	11.4
	20	3.0	229	7.64	2.16	13.7	2771	92.4	26.1	13.7
	30	3.0	335	11.20	3.16	16.3	2665	88.8	25.1	16.3
	40	3.0	447	14.90	4.21	18.4	2553	85.1	24.1	18.4
20	10	2.9	132	4.40	1.20	9.9	2868	95.6	25.3	9.9
	20	3.0	218	7.30	2.10	13.4	2782	92.7	26.2	13.4
27	1	5.2	43	1.43	1.22	18.4	2957	98.5	83.7	18.4
	5	3.5	79	2.63	1.01	11.2	2921	97.4	37.5	11.3
	10	3.0	159	5.30	1.50	11.6	2839	94.7	26.8	11.6
	15	3.0	233	7.70	2.20	13.8	2765	92.2	26.1	13.8
	20	3.0	288	9.60	2.70	15.2	2703	90.1	25.5	15.4
	40	3.2	454	15.10	4.90	21.0	2477	82.5	26.6	22.2

[a] In all cases the HO molecule was in its vibrational ground state.

TABLE 2: Summary of the Trajectory Calculations Which Led to Other Products

		$H + O_3$				$H + O_2 + O$				HO + O + O			
v''	E_{tr} (kcal mol^{-1})	N_r	P_r	σ^r/Å^2	$\Delta\sigma^r$/Å^2	N_r	P_r	σ^r/Å^2	$\Delta\sigma^r$/Å^2	N_r	P_r	σ^r/Å^2	$\Delta\sigma^r$/Å^2
27	20	5	0.0017	0.047	0.021	4	0.0013	0.038	0.019				
27	40	28	0.0093	0.300	0.056	32	0.0107	0.343	0.060	9	0.003	0.096	0.032

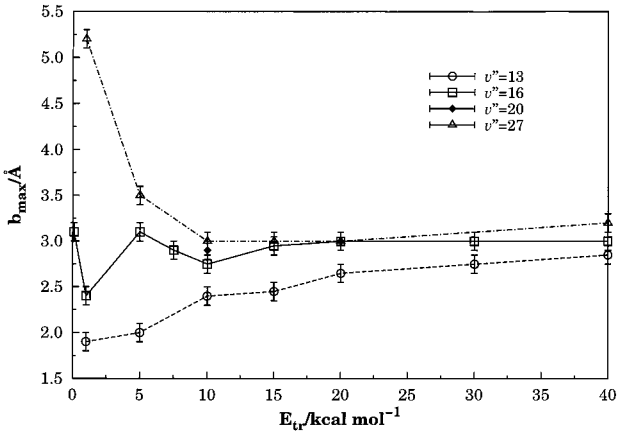

Figure 3. Energy dependence of the maximum impact parameter for the title reaction.

of a reaction with a threshold energy. Such a dependence of b_{max} on E_{tr} may therefore be rationalized as follows. The dominant interaction between HO and O_2 is, at large distances, of the dipole−quadrupole electrostatic type. Since the O_2 molecule is vibrationally excited (and this stretching leads to an increase of its electric quadrupole moment), one may then expect a more attractive long-range interaction. This may explain why b_{max} increases with decreasing translational energy. Conversely, for high translational energies, long-range forces are less important with translational energy in the reactive channel leading only to a small increase in b_{max}.

Figure 4a,b shows the opacity functions (*i.e.*, the reactive probability vs impact parameter) for low and high translational energies, and some vibrational combinations. For clarity only, the cases of $E_{tr} = 0.1$ kcal mol^{-1} ($v'' = 16$) and $E_{tr} = 1.0$ kcal

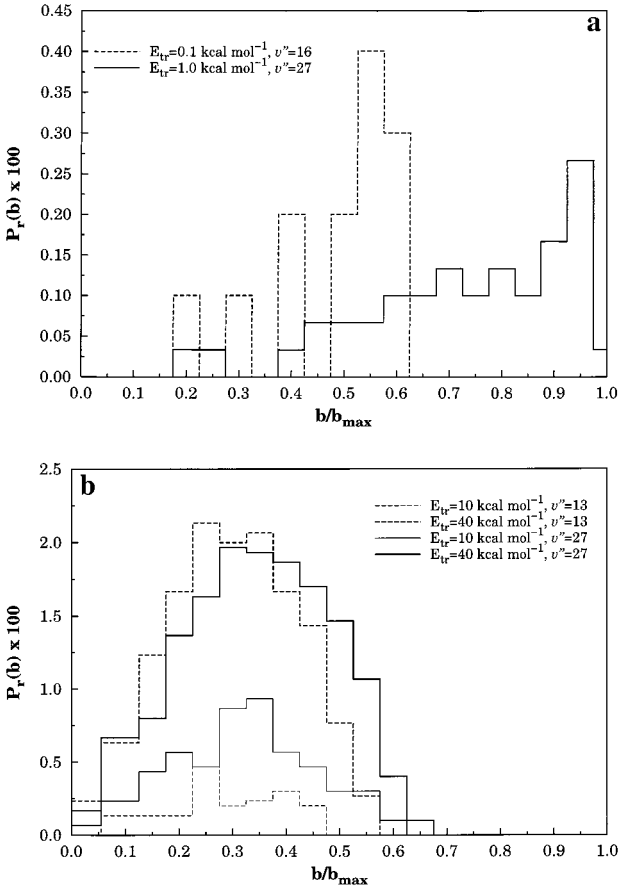

Figure 4. Opacity function for formation of HO_2: (a) capture-type regime; (b) barrier-type regime.

mol^{-1} ($v'' = 27$) are shown in Figure 4a, while in the high translation energy cases, they have been selected to show the typical shape and order of magnitude of the reactive probabilities. Note that the abcissae in these plots are b/b_{max}, with b_{max} being the largest impact parameter found for all batches that were run in the present work (5.2 Å). The notable feature from these figures is perhaps the fact that the opacity function shows two different patterns. For high translational energies, the opacity function has a bell shape (more common for reactions that have a threshold energy), while for low translational energies, it increases with impact parameter showing the effect of long-range forces. This can be explained as follows. First, one expects[25] a fall-off in reactivity with increasing impact parameter since, for a fixed translational energy, this would lead to an increase of the centrifugal barrier. On the other hand, as it has already been pointed out (note that the O_2 molecule is vibrationally excited, and hence has an increased electric quadrupole moment), long-range forces lead us to expect an increase of reactivity for large impact parameters. It is from this balance that the shape of the opacity function is defined at large values of *b*. For small *b* values, the small reactivity may be explained from the overlap of the electronic densities of the interacting species, which is likely to lead on average to an increase of the repulsive forces, at least over the investigated range of translational energies. The bell shape of the opacity functions for higher collisional energies may be similarly rationalized from the effects associated with translational energy (taking in consideration also the highly repulsive character of the regions of the potential energy surface sampled by the low-impact collisions), and height of the centrifugal barrier.

Figure 5 shows interatomic distance vs time plots for typical trajectories leading to formation of HO_2 in the "capture-type" and "barrier-type" regimes (these are defined from the shape of the associated excitation function, *i.e.*, σ_r vs E_{tr} curves to be discussed later), with examples being given of short-lived and long-lived trajectories. Clearly, on an average sense, long-lived trajectories are more likely expected to occur in the capture-type regime.

As a model to evaluate the average lifetime of the complex, we have defined the latter as a species in which all atomic distances were smaller than 1.36 times the largest interatomic distance in the geometry corresponding to equilibrium HO_3.[24] Thus, a complex has been assumed to be formed whenever all interatomic distances are smaller than that distance, and to cease to exist whenever one of the interatomic distances exceeded such a value without returning to it. Clearly, this definition of complex is seen from Figure 5 to mimic well what is obtained in the corresponding distance vs time plots. We also note from the displayed trajectories that the reaction tends to proceed by breaking the O_2 bond; *i.e.*, the oxygen atom of HO attacks one of the atoms of O_2 to form nascent HO_2 radicals.

Using the above definition of complex, we have estimated the average lifetime of the HO_3 complexes for a typical capture-type ($O_2(v{=}27)$, $E_{tr} = 1$ kcal mol^{-1}) process to be 0.226 ps, while for the barrier-type process ($O_2(v{=}13)$, $E_{tr} = 10$ kcal mol^{-1}) it was 0.128 ps. Similar results have been obtained for the corresponding capture regime in the studies of refs 25 and 31. Note that the complex lifetimes estimated in the present work are sufficient to allow many oscillations in the vibrational modes of the complex, thus warranting the possibility of internal energy exchange.

Figure 6 shows the scattering angle distribution for the combination (0,27) and several translational energies, while Table 3 gives its average value. It is seen that this decreases

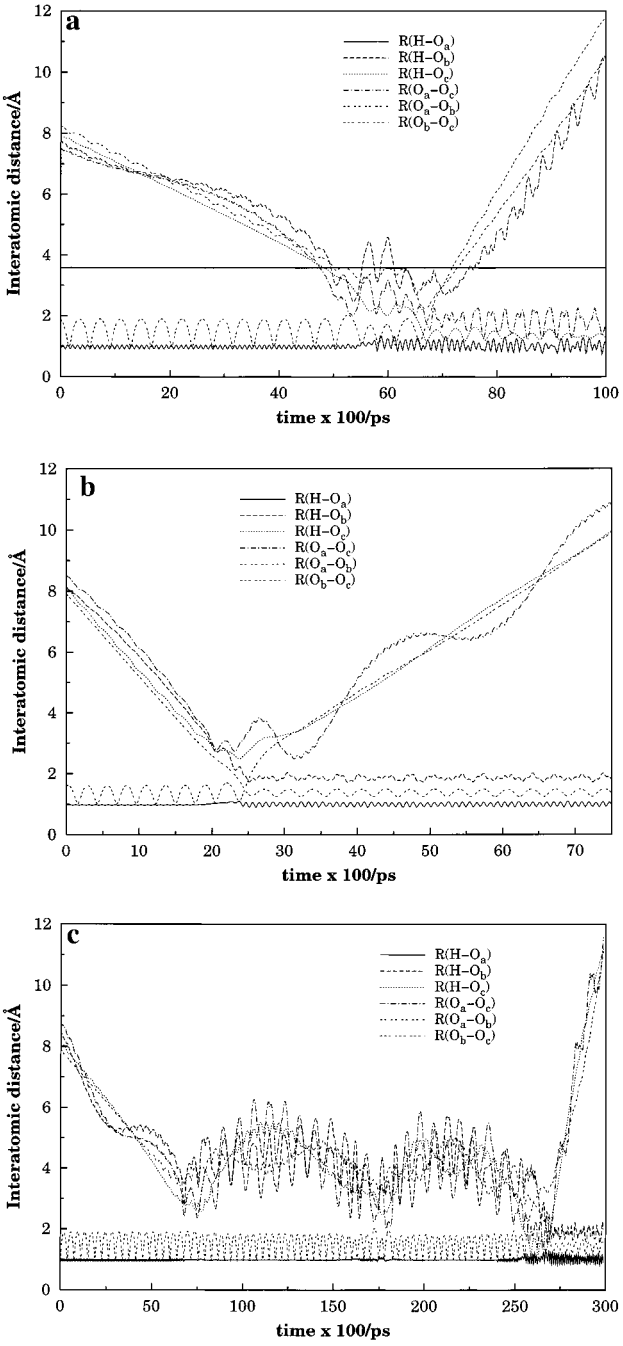

Figure 5. Typical distance vs time plots for the title reaction: (a) and (b) barrier- type regime ($v'' = 13$, $E_{tr} = 10$ kcal mol^{-1}); (c) capture-type regime ($v'' = 27$, $E_{tr} = 1$ kcal mol^{-1}). In panel (a), the thick line indicates the border distance for definition of complex (see the text).

with increasing translational energy, a result which may be explained from the fact that the complex lifetime decreases with translational energy. Such a result is also corroborated from the impact parameter vs E_{tr} curve. In fact, for $E_{tr} = 1$ kcal mol^{-1}, the number of reactive trajectories increases with impact parameter (Figure 4a) which is largest (5.2 Å) for this energy. As a result, the scattering angle is expected to be small on average. A corresponding analysis may be used to rationalize the values of $\langle\theta_{scatt}\rangle$ for other translational energies and vibrational combinations.

4.2. Energetic Features. Figure 7 shows the products energy distribution for the vibrational combination (0,27) and initial translational energies 1, 10, and 40 kcal mol^{-1}. Clearly, the outcoming HO_2 molecules have a considerable internal energy

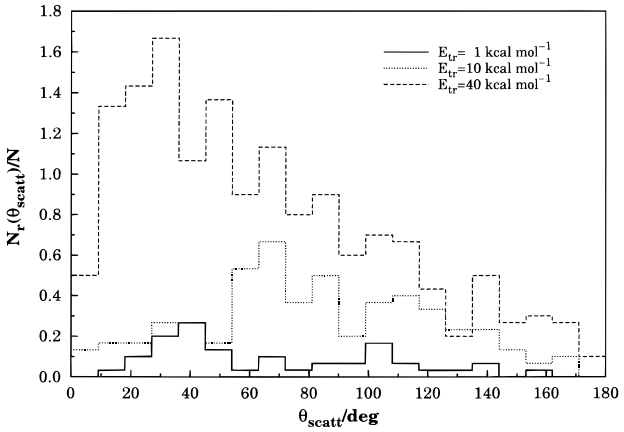

Figure 6. Scattering angle distribution for the combination (0,27) and several translational energies.

TABLE 3: Average Value of the Scattering Angle for Some Combinations of Vibrational Quantum Numbers of O_2 Molecule and Translational Energies

(v', v'')	E_{tr}/kcal mol^{-1}	$\langle\theta_{scatt}\rangle$
(0,17)	1	113.00
	10	82.41
	30	73.26
	40	70.04
(0,27)	1	68.06
	5	90.76
	10	81.80
	15	78.65
	40	65.03

content, with a significant part of it being in the rotational degrees of freedom. Thus, part of the translational and vibrational energies in the reactants has been converted to rotational energy in the products.

The product energy distributions for the translational and rotational degrees of freedom are also qualitatively similar for all values of E_{tr}. This observation may be rationalized from the fact that most of the relative translational energy is initially used to overpass the potential energy barrier. Since, immediately before formation of the complex, both the translational and rotational degrees of freedom are likely to have been reduced to a minimum amount, it is reasonable to expect that similar distributions may also be observed in the exit channel. Indeed, a similar trend is found for other initial vibrational combinations (not shown).

The partitioning of the energy release in the product molecules is also shown in Table 4. As expected from the analysis of Figure 7, we find similar average values for the translational and rotational energies which are obtained as usual from the code output. The notable feature is perhaps the fact that the average value of the vibrational energy of the HO_2 radical represents more than half of the total energy of the products. It is also interesting to note that the distributions shown in Table 4 are very similar for 1 and 10 kcal mol^{-1}, although these translational energies correspond to two different regimes (capture-type and barrier-type). Note that, except for the lowest translational energies and vibrational combinations (0, 13) and (0, 16), the average vibrational energy of the product HO_2 molecules is higher than the corresponding zero-point energy[32] of the triatomic (5.4 kcal mol^{-1}). However, somewhat unexpected, a significant fraction of the nonreactive trajectories leads to an HO molecule with an energy below its zero-point value (1.484 kcal mol^{-1}). Thus, although we may safely ignore in the present study the problem of zero-point energy leakage (for

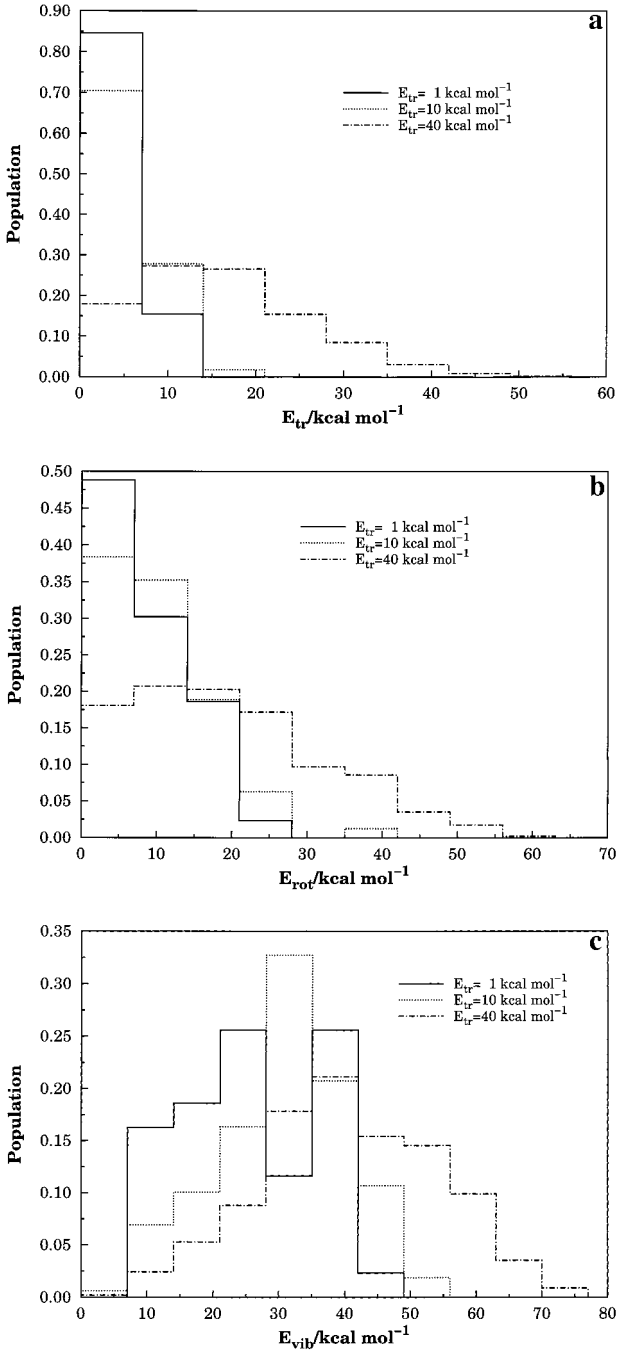

Figure 7. Energy distributions in the products for HO_2 formation: (a) translational; (b) rotational, and (c) vibrational energy.

a few references on this issue, see refs 33−39) in the reactive trajectories, this is not quite so if all trajectories are considered. Indeed, about 20−30% of the nonreactive HO species end up below its zero-point energy value. If one assumes that some of these trajectories become reactive when the flow of energy in the vibrational modes is constrained to keep at least its minimum energy content, then we may say that the calculated reactivities are probably underestimated. An answer to this problem has to await until quantum dynamical calculations are carried out for the title reaction.

In Figure 8 we show the vibrational−rotational distribution of HO_2 for the vibrational combination (0,27) at two distinct energies (1 and 10 kcal mol^{-1}). The dash-dotted line indicates the threshold energy for dissociation of HO_2 into HO + O. In turn, the dashed lines correspond to $E_{vib} + E_{rot} = \langle E_{vib} + E_{rot}\rangle$ while the solid ones refer to $E_{vib} + E_{rot} = \langle E_{vib} + E_{rot} + E_{tr}\rangle$.

TABLE 4: Percentages of Energy Partitioned to Different Degrees of Freedom for the Reaction HO(0) + $O_2(v'')$ → HO_2 + O

v''	E_{tr} (kcal mol^{-1})	$\langle E_{tr}\rangle$ (kcal mol^{-1})	$\langle E_{tr}\rangle$ (%)	$\langle E_{tr}\rangle$ (kcal mol^{-1})	$\langle E_{tr}\rangle$ (%)	$\langle E_v\rangle$ (kcal mol^{-1})	$\langle E_v\rangle$ (%)
13	10	3.87	21.2	4.70	25.8	9.66	53.0
	40	14.60	30.8	11.61	24.5	21.24	44.8
16	1	3.46	20.4	3.84	22.6	9.69	57.0
	10	5.70	21.3	6.45	24.2	14.61	54.5
	40	16.45	29.4	13.93	24.9	25.52	45.7
27	1	9.77	21.2	9.14	21.2	25.66	57.8
	5	10.18	21.0	9.82	20.4	28.49	58.8
	10	11.70	22.1	10.41	19.5	31.00	58.4
	15	12.63	21.7	11.55	19.9	33.78	58.5
	40	21.86	26.9	19.71	23.6	40.74	49.5

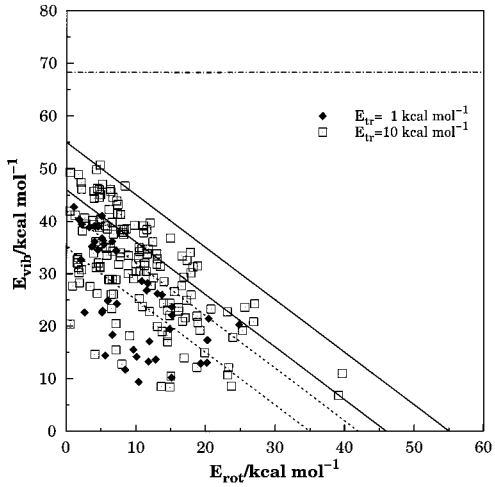

Figure 8. Vibrational−rotational energy partition in the product HO_2 molecules. The dash-dotted line indicates the threshould energy for dissociation into HO + O. See also text.

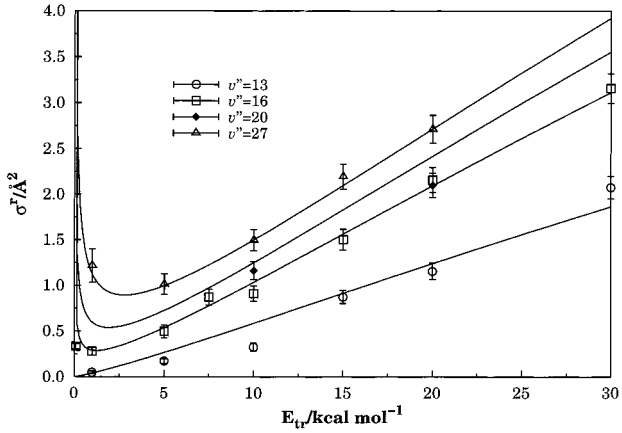

Figure 9. Figure 9: Reactive cross section sr as a function of the translational energy for HO2 formation. Also indicated are the 68error bars and the fitted lines given by eq 13.

Of course, in both cases, all points must lie below the line associated to $E_{vib} + E_{rot} = \langle E_{vib} + E_{rot} + E_{tr}\rangle$ (they should form a microcanonical ensemble if they all lied on the displayed dashed straight line).

4.3. Reactive Cross Section. We now examine the shape of the excitation functions (cross section vs translational energy) which are shown in Figure 9 together with the associated 68% error bars for formation of HO_2 + O. There are two opposite trends which explain their shapes. At low energies, the capture-type regime dominates leading to the well established (*e.g.*, refs 25, 31, 40, and references therein) decreasing dependence of σ^r with E_{tr}. At high energies, one observes the common pattern found in reactions which have an energy threshold; *i.e.*, σ^r is an increasing function of E_{tr}. As a result, the excitation function shows a minimum in the region where the two effects balance each other.

To investigate the effect of rotation, we have carried out calculations at two translational energies by choosing the reactants, for the vibrational combination (0,27), to be in the rotational states $j_{HO} = 10^{27}$ and $j_{O_2} = 9^{41}$ (which correspond approximately to their optimum populations). The calculated cross sections are, for $E_{tr} = 10$ and 40 kcal mol^{-1}, respectively, $\sigma^r = 3.2$ Å^2 and $\sigma^r = 5.1$ Å^2. Moreover, we have calculated a cross section for $E_{tr} = 40$ kcal mol^{-1}, considering only the rotation in O_2; the result was $\sigma^r = 3.3$ Å^2. Clearly, the inclusion of rotational excitation in HO has a significant effect on the reactive probability only at low energies. This is probably due to (primarily) an increase of the available energy content and orientational effects, with the latter being expected to be more relevant at low energies since the molecules have then time to reorient and find the optimum orientation for reaction. This issue will hopefully be explored in further detail in future work.

To analytically describe the dependence of the cross section with the translational energy, we have adopted the form

$$\sigma^r_{0v''} = C\frac{(v'' - v_{th})}{E^n_{tr}} + B_{v''}E^{6/5}_{tr}\exp(-mE_{tr}) \qquad (13)$$

where v_{th} is a threshold vibrational quantum number, $m = 0.008$ (kcal mol^{-1})$^{-1}$ is a decay factor (assumed to be constant for all cases), and the coefficient $B_{v''}$ is a function of the vibrational quantum number. Note that the power of E_{tr} in the capture-type contribution (*i.e.*, the first term in eq 13) has been fixed at $n = {}^1/_2$, which may be justified from the values expected for the E_{tr} dependence of the cross section in the case of a dipole−quadrupole interaction (*i.e.*, $n = {}^2/_4$). For $B_{v''}$ we have assumed a Taylor series expansion up to the fifth order around $v'' = 13$, namely

$$B_{v''} = \sum_{k=0}^{4} b_k(v'' - 13)^k \qquad (14)$$

with the parameters C and b_k being determined from a least-squares fitting procedure; their optimum numerical values are reported in Table 5. The fitted functions are shown together with the calculated points in Figure 9. It is seen that eq 13 reproduces well the calculated points. Also shown in this figure is the curve for $v'' = 20$, and the two calculated points for $E_{tr} = 10$ and 40 kcal mol^{-1} (not fitted) for this vibrational combination provide a test of the above analytical expression. Although there are only a few calculated points for very low energies due to their high computational cost, the calculated ones seem sufficient to highlight the involved trends.

TABLE 5: Optimum Numerical Values for the Parameters of $\sigma^r_{0v''}$[a]

C	0.0745872
b_0	0.04
b_1	0.0099
b_2	0.000001
b_3	−0.000169
b_4	0.0000095

[a] The units are such that the energy is in kcal mol^{-1} and cross section in Å^2.

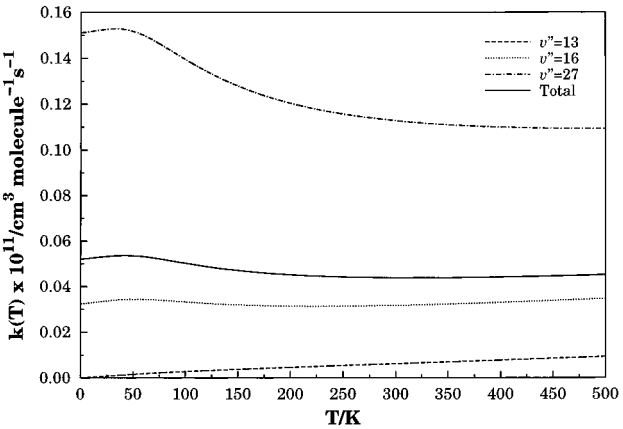

Figure 10. Specific and averaged thermal rate coefficients for the title reaction.

By substitution of eq 13 in eq 8 and performing the integration analytically, the specific thermal rate coefficient $k_{0v''}(T)$ assumes the form

$$k_{0v''}(T) = g_e(T)\left(\frac{2}{k_B T}\right)^{3/2}\left(\frac{1}{\pi\mu}\right)^{1/2}\left[C_{v''}(k_B T)^{3/2}\,\Gamma(3/2) + B_{v''}\frac{\Gamma(16/5)}{(0.008 + (1/k_B T))^{16/5}}\right] \quad (15)$$

where $C_{v''} = C(v'' - 13)$ and $\Gamma(...)$ is the gamma function. Figure 10 shows the function in eq 15 for vibrational quantum numbers 13, 16, and 27 of the oxygen molecule. A simple algebraic analysis shows that, for $T \ll 1/0.008k_B$, eq 15 can be approximately expressed as

$$k_{0v''}(T) = g_e(T)\left(\frac{8}{\pi\mu}\right)^{1/2}\left[C_{v''}\Gamma(3/2) + B_{v''}\Gamma(16/5)\,(k_B T)^{17/10}\right] \quad (16)$$

which should therefore be valid for most temperature regimes of practical interest. Moreover, from eq 16, one has

$$\lim_{T\to 0} k_{0v''}(T) = \frac{1}{3}\left(\frac{8}{\pi\mu}\right)^{1/2} C_{v''}\Gamma(3/2) \quad (17)$$

For very high temperatures, $T \gg 1/0.008k_B$, one obtains

$$k_{0v''}(T) = g_e(T)\left(\frac{8}{\pi\mu}\right)^{1/2}\left[C_{v''}\Gamma(3/2) + B_{v''}\frac{\Gamma(16/5)}{(0.008)^{16/5}\,(k_B T)^{3/2}}\right] \quad (18)$$

with the limit being

$$\lim_{T\to\infty} k_{0v''}(T) = \frac{1}{6}\left(\frac{8}{\pi\mu}\right)^{1/2} C_{v''}\Gamma(3/2) \quad (19)$$

Thus, the limits are essentially determined by the electronic degeneracy factor $g_e(T)$. This determines the increase of the specific rate constant for very small temperatures, a feature which may have importance in atmospheric chemistry at high altitudes. For completeness, we also show in Figure 10 the vibrationally averaged thermal rate coefficient

$$k(T) = \frac{\sum_{v''}\omega_{v''}k_{0v''}(T)}{\sum_{v''}\omega_{v''}} \quad (20)$$

where the populations $\omega_{v''}$ for the vibrational state v'' have been assumed to be given by that obtained in the 226 nm photolysis of ozone.[42] Although having, of course, some influence on its magnitude, such averaging does not substantially alter the shape of the rate coefficient.

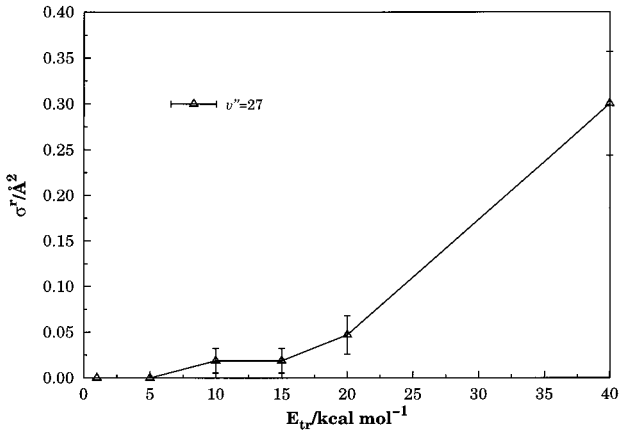

Figure 11. Reactive cross section σ^r as a function of the translational energy for ozone formation. Also indicated are the 68% error bars.

4.4. Other Reactive Channels. Table 2 summarizes the results obtained for other reactive channels when the vibrational quantum number of the oxygen molecule is $v'' = 27$. As seen, such channels have a small reactive cross section. Of particular interest is the channel that leads to ozone formation. Clearly, this process becomes relevant only at high translational energies, as shown in Figure 11. In this case, the extra calculations done for rotational quantum numbers $j_{HO} = 10$ and $j_{O_2} = 9$ show that the addition of rotational energy also enhances the formation of such products, especially in the high translational energy regime. This is most likely due to the increase of the available energy content, since orientational effects are expected to be less important at the high energies of relevance in this section (*i.e.*, the molecules do not have time to reorient and find the optimum orientation for reaction).

5. Conclusions

In spite of its importance, the title multichannel reaction has not been studied so far theoretically due to lack of a realistic potential energy surface. Our motivation in this work has been to cover this gap and hence initiate a series of studies using a DMBE potential energy surface for the ground doublet state of HO_3 recently proposed by one of us.[24] Specifically, we have carried out here a QCT study of the reaction HO + O_2 for the vibrational combinations ($v' = 0$, v''). The calculations have shown that it occurs for vibrational quantum numbers larger than $v'' = 13$ over the whole range of translational energies. In most cases, no breaking of the HO bond takes place. It has also been shown that the product HO_2 radical is formed with a substantial amount of internal energy, both rotational and vibrational. Moreover, the calculations suggest that the title reaction occurs both via capture-type and barrier-type mecha-

nisms, for low and higher translational energies, respectively. Finally, the calculations carried for the combination of rotational quantum numbers ($j_{HO} = 10$, $j_{O_2} = 9$) and for the combination ($j_{HO} = 10$, $j_{O_2} = 1$) suggest that the rotational excitation of the HO may play a significant role both for the formation of HO_2 and O_3. We plan to explore such effects as well as the reaction leading to ozone formation in a future publication. Finally, we should mention that no comparison with experimental data was possible since, to our knowledge, no such data exists in the literature. We hope that the present study may stimulate such work especially using laser techniques which allow the preparation of vibrationally hot reactant molecules. Through such techniques, it may be possible to control the outcomes of the title reaction.

Acknowledgment. This work has the support of Fundação para a Ciência e Tecnologia, Portugal, under programs PRAXIS XXI an FEDER (Contract 2/2.1/QUI/408/94).

References and Notes

(1) Bates, D. R.; Nicolet, M. *J. Geophys. Res.* **1950**, *55*, 301.
(2) McDade, J. C.; Llewellyn, E. *J. Geophys. Res.* **1987**, *92*, 7643.
(3) Steinfeld, J. I.; Francisco, J. S.; Hase, W. L. *Chemical Kinetics and Dynamics*; Prentice Hall: Englewood Cliffs, NJ, 1989.
(4) Downey, G. D.; Robinson, D. W.; Smith, J. *J. Phys. Chem.* **1977**, *66*, 1685.
(5) Charters, P. E.; Macdonald, R. G.; Polanyi, J. C. *Appl. Opt.* **1971**, *10*, 1747.
(6) Anlauf, K. G.; Macdonald, R. G.; Polanyi, J. C. *Chem. Phys. Lett.* **1968**, *1*, 619.
(7) Polanyi, J. C.; Sloan, J. J. *Int. J. Chem. Kinet. Symp.* **1975**, *1*, 51.
(8) Keyser, L. F. *J. Phys. Chem.* **1979**, *83*, 645.
(9) Clyne, M. A. A.; Monkhouse, P. B. *J. Chem. Soc., Faraday Trans. 2* **1977**, *73*, 298.
(10) Phillips, L. F.; Schiff, H. I. *J. Chem. Phys.* **1962**, *37*, 1233.
(11) Lee, J. H.; Michael, J. V.; Payne, W. A.; Stief, L. J. *J. Chem. Phys.* **1978**, *69*, 350.
(12) Greenblatt, G. D.; Wiesenfeld, J. R. *J. Geophys. Res.* **1982**, *87*, 11145.
(13) Finlayson-Pitts, B. J.; Kleindienst, T. E.; Ezell, M. J.; Toohey, D. W. *J. Chem. Phys.* **1981**, *74*, 4533.
(14) Washida, N.; Akimoto, H.; Okuda, M. *J. Chem. Phys.* **1980**, *72*, 5781.
(15) Finlayson-Pitts, B. J.; Kleindienst, T. E. *J. Chem. Phys.* **1979**, *70*, 4804.
(16) Howard, C. J.; Finlayson, B. J. *J. Chem. Phys.* **1980**, *72*, 3842.
(17) Force, A. P.; Wiesenfeld, J. R. *J. Chem. Phys.* **1981**, *74*, 1718.
(18) Ohoyama, H.; Kasai, T.; Yoshimura, Y.; Kuwata, H. *Chem. Phys. Lett.* **1985**, *118*, 263.
(19) Zuhrt, C.; Zülicke, L.; Umansky, S. Y. *Chem. Phys.* **1986**, *105*, 15.
(20) Zuhrt, C.; Zülicke, L. *Chem. Phys. Lett.* **1984**, *111*, 408.
(21) Shalashilin, D. V.; Umanskii, S. Y.; Gershenzon, M. *Chem. Phys.* **1992**, *95*, 315.
(22) Dodd, J. A.; Lipson, S. I.; Blumberg, W. A. M. *J. Chem. Phys.* **1991**, *95*, 5752.
(23) Shalashilin, D. V.; Michtchenko, A. V.; Umanskii, S.; Gershenzo, Y. M. *J. Phys. Chem.* **1995**, *99*, 11627.
(24) Varandas, A. J. C.; Yu, H. G. *Mol. Phys.* **1997**, *91*, 301.
(25) Wang, W.; González-Jonte, R.; Varandas, A. J. C. *J. Phys. Chem.* **1998**, *102*, 6935.
(26) Varandas, A. J. C.; Szichman, H. *Chem. Phys. Lett.* **1998**, *295*, 113.
(27) Yu, H. G.; Varandas, A. J. C. *J. Chem. Soc., Faraday Trans.* **1997**, *93*, 2651.
(28) Szichman, H.; Baer, M.; Varandas, A. J. C. *J. Phys. Chem.* **1997**, *101*, 8817.
(29) Szichman, H.; Varandas, A. J. C. *J. Phys. Chem.* **1999**, *103*, 1967.
(30) Hase, W. L. MERCURY: a general Monte-Carlo classical trajectory computer program, QCPE#453. An updated version of this code is VENUS96: Hase, W. L.; Duchovic, R. J.; Hu, X.; Komornik, A.; Lim, K. F.; Lu, D.-H.; Peslherbe, G. H.; Swamy, K. N.; van de Linde, S. R.; Varandas, A. J. C.; Wang, H.; Wolf, R. J. *QCPE Bull.* **1996**, *16*, 43.
(31) Marques, J. M. C.; Wang, W.; Pais, A. A. C. C.; Varandas, A. J. C. *J. Phys. Chem.* **1996**, *100*, 17513.
(32) Varandas, A. J. C.; Bowman, J. M.; Gazdy, B. *Chem. Phys. Lett.* **1995**, *233*, 405.
(33) Varandas, A. J. C. *Chem. Phys. Lett.* **1994**, *225*, 18.
(34) Varandas, A. J. C.; Marques, J. M. C. *J. Chem. Phys.* **1994**, *100*, 1908.
(35) Kumar, S.; Sathyamurthy, N.; Ramaswamy, R. *J. Chem. Phys.* **1995**, *103*, 6021.
(36) Ben-Nun, M.; Levine, R. D. *J. Chem. Phys.* **1996**, *105*, 8136.
(37) Guo, Y.; Thompson, D. L.; Sewell, T. D. *J. Chem. Phys.* **1996**, *104*, 576.
(38) Lim, K. F. *J. Chem. Soc., Faraday Trans.* **1997**, *93*, 669.
(39) Marks, A. J. *J. Chem. Phys.* **1998**, *108*, 1438.
(40) Varandas, A. J. C. *Faraday Discuss. Chem. Soc.* **1987**, *84*, 353.
(41) Varandas, A. J. C.; Wang, W. *Chem. Phys.* **1997**, *215*, 167.
(42) Miller, R. L.; Suits, A. G.; Houston, P. L.; Toumi, R.; Mack, J. A.; Wodtke, A. M. *Science* **1994**, *265*, 1831.